Heavy-Ion Broad-Beam and Microprobe Studies of Single-Event Upsets in 0.20-μm SiGe Heterojunction Bipolar Transistors and Circuits

Robert A. Reed, *Member, IEEE*, Paul W. Marshall, *Member, IEEE*, James C. Pickel, *Fellow, IEEE*,
Martin A. Carts, *Member, IEEE*, Bryan Fodness, *Member, IEEE*, Guofu Niu, *Senior Member, IEEE*,
Karl Fritz, Gyorgy Vizkelethy, *Member, IEEE*, Paul E. Dodd, *Member, IEEE*, Tim Irwin, *Member, IEEE*,
John D. Cressler, *Fellow, IEEE*, Ramkumar Krithivasan, *Student Member, IEEE*, Pamela Riggs, Jason Prairie,
Barbara Randall, Barry Gilbert, *Fellow, IEEE*, and Kenneth A. LaBel, *Member, IEEE*

Abstract—Combining broad-beam circuit level single-event upset (SEU) response with heavy ion microprobe charge collection measurements on single silicon-germanium heterojunction bipolar transistors improves understanding of the charge collection mechanisms responsible for SEU response of digital SiGe HBT technology. This new understanding of the SEU mechanisms shows that the right rectangular parallele-piped model for the sensitive volume is not applicable to this technology. A new first-order physical model is proposed and calibrated with moderate success.

Index Terms—Ground testing, modeling, SiGe, silicon germanium, single event effect, single event upset.

I. INTRODUCTION

SILICON-GERMANIUM (SiGe)-based technology is widely recognized for its potential to impact the high-speed microelectronic industry by monolithic incorporation of low-power complementary logic with extremely high-speed SiGe heterojunction bipolar transistor (HBT) logic. This BiCMOS approach exploits the maturity of the silicon fabrica-tion industry where large scale integration and high yields are possible. Consequently, the satellite industry stands to benefit from insertion of both COTS and custom designs. This is espe-cially true in signal processing and data handling applications where RF elements are combined with high bandwidth routing of digital signals along with lower bandwidth processing. A va-riety of studies have examined the ionizing dose, displacement damage, and single event characteristics for devices fabricated in IBM SiGe HBT process [1 and references therein].

Accessibility to SiGe through an increasing number of man-ufacturers adds to the importance of understanding its intrinsic radiation characteristics, and in particular the single-event effect (SEE) characteristics of the high bandwidth HBT-based circuits. IBM is now manufacturing its second generation of their com-mercial SiGe HBT processes, and access is currently available to the first generation HBT (known as 5HP and 6HP) through the MOSIS [2] shared mask services with anticipated future re-lease of the latest (7HP) process. The 5HP process is described in [1 and references therein] and is characterized by a minimum feature size (emitter spacing) of 0.5 μm and a cut-off frequency f_T of 50 GHz, whereas the fully scaled 7HP HBT employs a 0.20 μm emitter and has an f_T of 120 GHz (the PRN used for this work was manufactured in a 90-GHz f_T version of 7HP).

Previous investigations have examined SEE response of 5HP HBT circuits through both circuit testing [3] and modeling [4]–[6]. Charge collection modeling [7], [8] and measurement [8] studies in the 5HP process have also been conducted, but to date no measurements have been reported on charge collection or circuit response in 7HP SiGe HBT structures. Nor have circuit models for charge collection been developed in any version other than the 5HP HBT structure.

Our investigation reports the first results for both charge col-lection and circuit response in IBM's 7HP-based SiGe process. We compare broad-beam heavy-ion single-event upset (SEU) test results in a fully functional pseudorandom number (PRN) sequence generator for frequencies up to 12 Gbps versus effec-tive linear energy transfer (LET). We also report proton test re-sults in the same circuit. In addition, we examine the charge collection characteristics of individual 7HP HBT structures and map out the spatial sensitivities using the Sandia National Lab-oratory microbeam facility's Ion Beam Induced Charge Collec-tion (IBICC) technique [9]. Combining the two data sets offers
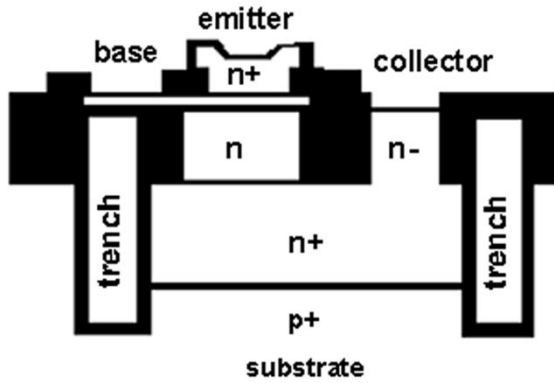
Fig. 1. Drawing of HBT device cross section [after [1]].

insights into the charge collection mechanisms responsible for circuit level SEU response and provides the first insights into the SEU characteristics of this latest version of IBM's commercial SiGe process.

We also present a new first-order model of the charge collection processes in deep trench isolated SiGe HBT devices (this development was motivated by the failure of existing physical models). This model is an extension of the model we presented in [11] for modeling charge collection processes in imagers. The intent of this modeling is to eventually develop an improved on-orbit SEU rate prediction method for IBM SiGe HBT technology.

II. OVERVIEW OF IBM'S 0.20-μm SiGe HBT

Fig. 1 shows a diagram of the physical layout of an IBM SiGe HBT and identifies the location of the base, emitter, and collector contacts [after [1]]. The transistor is manufactured almost entirely from silicon; the only germanium used is a small fraction of the material confined in the base region. The transistor area is totally contained inside two insulating trenches—a shallow trench (not indicated in the figure) and a deep trench.

The next set of bullets list the portions of the HBT structure that are of particular interest for the studies described in this paper.

- A 7 μm long, 1 μm wide isolation trench completely surrounds the transistor. We will call this the "trench volume." The "trench area" is the "top" area of the trench (i.e., the closet to the metallization).
- The substrate-collector junction (SCJ) is defined by the n^+p^+ interface 5 μm below the silicon-metallization layer interface.
- The volume of silicon that is confined on four sides by the deep isolation trench, with its top defined by the silicon-metallization layer interface, and its bottom defined by the SCJ will be called "active volume." The "active area" is the area for this volume that is normal to the top of the die surface—note that the collector volume makes up most of this volume.
- The substrate is defined as the silicon that lies outside the active and trench volume (we will call this the "substrate volume").
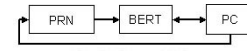

Fig. 2. Block diagram of PRN test setup.

III. BROADBEAM TESTING OF A 7HP PRN SEQUENCE GENERATOR

A. Test Circuit Description and Test Methods

The device was a $2^7 - 1$ PRN sequence generator fabricated in IBM 0.20-μm, $f_T = 90$ GHz (7HP) SiGe process. It was designed by the Special Purposes Processor Group (SPPG) at Mayo Foundation and fabricated by IBM. It consists of seven flip-flops in series, with the output of the last two stages XORed and fed back to the input of the first stage. All permutations of states of the seven flip-flops are generated, except all zeros (referred to as the "zero state"), giving a sequence of 127 bits known as 7-bit PSR number sequence. The device is capable of producing digital data streams between 200 Mbps and 12 Gbps.

The device under test (DUT) has two truly differential inputs, a clock signal (CLK and CLKbar) and a reset signal (R and Rbar) to help recover from the zero-state. High level for both is 0 V_{dc}. Low level for both is -0.3 V_{dc}. The single DUT output is also truly differential, with the same levels (mV_{pp} about -150 mV_{dc}).

The test setup reflects the operational needs of the PRN (especially handling 12.5 Gbps digital signals and providing a static-safe environment). Fig. 2 gives a simplified block diagram of the test setup. The heart of the test system is the Anritsu MP1764A, a 12.5-Gbps bit error rate tester (BERT) [12]. It provides error detection of the incoming PRN serial data stream, given a synchronizing clock signal and knowledge of the expected data.

The BERT was manually programmed to interrogate the incoming bit stream for errors. Nearly all errors in the data sequence will result in a loss of synchronization between the PRN and the BERT. When an error occurs the BERT passes an error flag to the control PC, which tallies the errors and resets the PRN. Errors are accumulated for each exposure and reset cross sections are computed.

B. Experimental Synchronization Error Results

Heavy ion testing of PRN was carried out at Texas A&M University Cyclotron Facility. These data represent the first measurement of the SEU sensitivity of a device fabricated in IBM 0.20-μm SiGe HBT.

In order to achieve the desired ion LETs with sufficient range into silicon we used a combination of neon at 40 MeV/amu, argon at 40 and 15 MeV/amu, and krypton at 15 MeV/amu. Testing was carried out using at least five angles of incidence: 0, 30, 45, 60, and 72 degrees. For all ions, the LET varies less than 14% over a distance of 45 μm.

Fig. 3 is a log-log plot of the cross section for PRN resets when exposed to heavy ions with various "effective" LETs. As is typically done for heavy ion exposures, the normal incidence fluence and LET have been corrected using the $\cos(\theta)$ laws that arise from beam angle of incidence considerations when exposing a thin rectangular parallelpiped (RPP) sensitive volume.
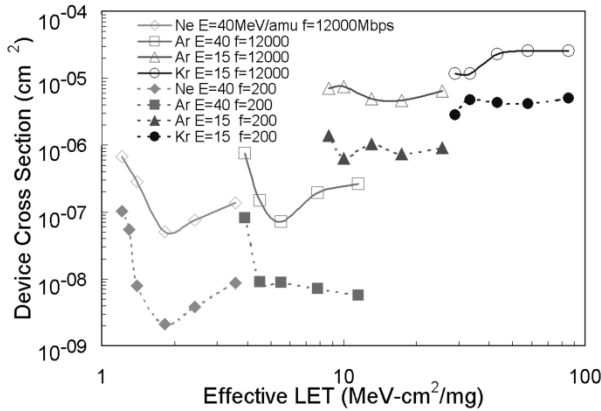
Fig. 3. Cross-section results on the PRN. Data are presented with angle of incidence correction for RPP.

Fig. 4. Proton and heavy ion cross-section measurements over operating frequency.

The data in Fig. 3 connected by solid lines (and unfilled symbols) are for a 12 Gbps serial data stream, those connected by the dashed lines (filled symbols) are for 0.2 Gbps. Each symbol type represents a different normal incident ion LET. Each solid or dashed line connects data taken at a single normal incident LET for 0, 30, 45, 60, and 70 degrees (an additional data point was taken at 15 degrees for Ne at 200 Mbps).

These data show that the threshold LET for this device is less than $1.2 \, \mathrm{MeV-cm^2/mg}$. This very low LET threshold for SEU is consistent with the data on the IBM 5HP [3].

Also note that data at both data rates in Fig. 3 show that the "effective" cross section decreases with increasing "effective" LET by nearly two orders of magnitude for low LET values (a result that is consistent with the SEU data on the IBM 5HP technology [3]). This demonstrates an anomalous response with angle of incidence. We will discuss this in more detail after we present the microbeam IBICC results.

Fig. 4 plots data trends over operating frequency for Ne and Kr ions. It also plots the trend of the cross section over frequency for 198 MeV protons—the proton tests were preformed at Indiana University using the same test setup used for heavy ion testing. The cross-section data show a slight increase with increasing frequency for $< 12 \, \mathrm{Gbps}$. The data show a large increase in the measured cross section when testing near the maximum operation frequency. These trends are consistent with similar trends measured on circuits fabricated in 5HP [3].

IV. MICROBEAM TESTING OF HBT TRANSISTORS

A. Test Circuit Description and Test Methods

Sandia National Laboratory's IBICC Facility [9] was used to interrogate the amount of charge collected by each terminal of a single SiGe 7HP HBT transistor.

The die used for microbeam testing had a single $0.18 \times 19.2 \, \mu\mathrm{m}^2$ transistor bonded out to a ceramic dual inline package (DIP). The active volume was $3 \times 20 \times 5 \, \mu\mathrm{m}^3$ (we will be using the terms defined in Section II to describe the device geometry). The isolation trench area is outlined by a $5 \times 22 \, \mu\mathrm{m}^2$ rectangle. (Recall the trench is $\sim 1 \, \mu\mathrm{m}$ wide and $7 \, \mu\mathrm{m}$ deep.)

The die was exposed to a chemical vapor etch process to remove any polyimide that was on top of the die. After etching there was approximately $7.6 \, \mu\mathrm{m}$ of dead layer (this was deter-
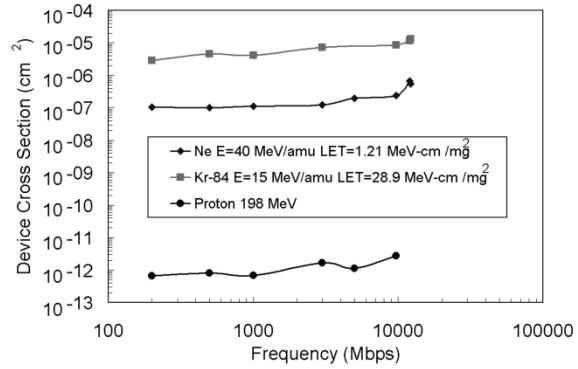
mined from SEM images) that consisted of several alternating metal/insulator layers plus passivation layers.

A four-probe IBICC measurement was used to simultaneously measure the charge induced on the Collector (C), Emitter (E), Base (B), and substrate (Sx) terminals due to ion strikes occurring in and around the transistor area. The test conditions were E,B,C grounded, Sx set to $-5.2 \, \mathrm{V}$.

The flux was set sufficiently low to ensure that no more than one ion was incident on the die at each step. The IBICC measurements were made using 36 MeV oxygen ions. The range of these ions in silicon is $24.5 \, \mu\mathrm{m}$, giving nearly $17 \, \mu\mathrm{m}$ of penetration in the device, which is sufficient to penetrate well into the substrate volume. For all tests the ion beam spot size was near $2 \, \mu\mathrm{m}^2$, this spot was stepped through a $1600\text{-}\mu\mathrm{m}^2$ area that contained the transistor with a step size of about $0.1 \, \mu\mathrm{m}$. The data cube is built up by several scans of the large area and consists of the location of the ion spot (X and Y coordinates) and the charge collected by each probe for each ion strike.

Forward and inverse Gummel plots were measured before and after each run in the bias condition range of interest, these postirradiation data showed no degradation of transistor performance.

A measure of the accuracy of the IBICC measurement technique is to determine the net charge collected on all contacts and properly account for the sign of the charge. Holes will be collected on the base and substrate while electrons will the collected on the collector and emitter [8]. For the data presented in this paper, over 90% of the events had less than 10% difference in the total charge collected via holes versus that for electrons. This shows that we have high confidence that the charge collection events are due to ions traversing the device and not a result of extraneous electrical noise.

B. Microbeam Results on IBM 0.20-$\mu\mathrm{m}$ HBT

Fig. 5(a) shows a three–dimensional (3-D) smoothed fit to the charge collection results obtained on the HBT collector. The collected charge (fC) is plotted as a function of $X(\mu\mathrm{m})$ and $Y(\mu\mathrm{m})$ position. The emitter contact showed no charge collection—all measurable electron charge collection appears on the collector.

The data in Fig. 5(a) show a well-defined charge collection area for events that produce more than 200 fC on the collector. The dimensions of this area are $5 \times 22 \, \mu\mathrm{m}^2$ and agrees with the sum of the active and trench areas. Events that produce less than 200 fC occur outside this well defined area.
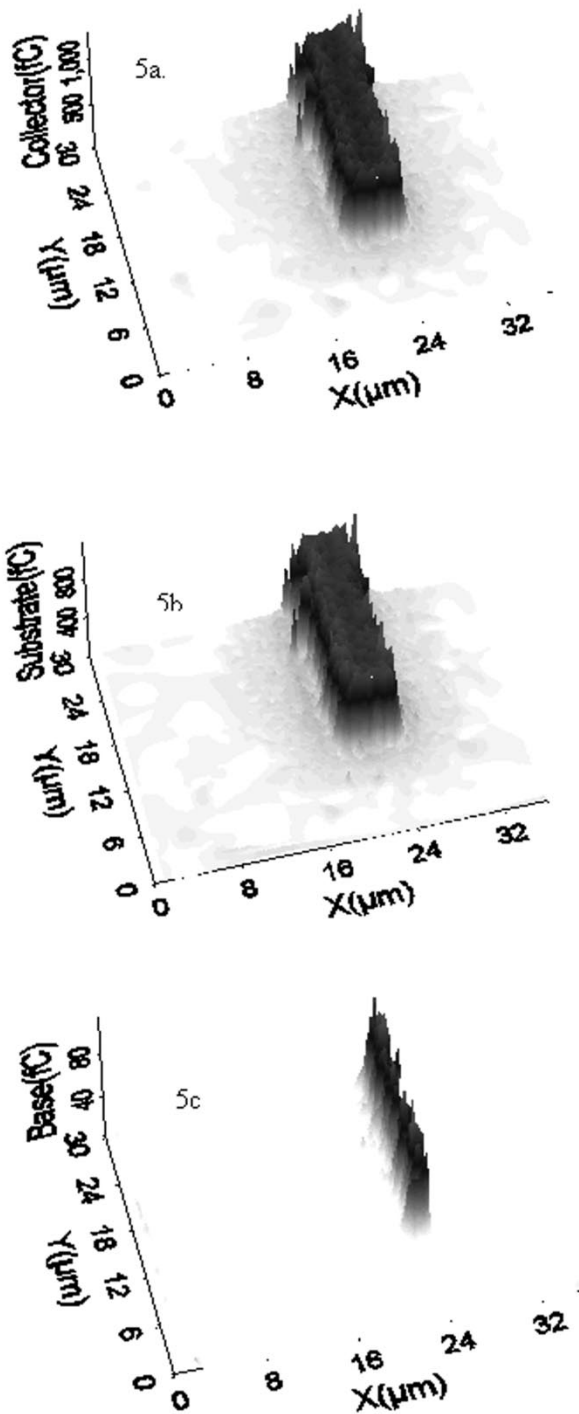
Fig. 5. IBICC measurement for (a) collector; (b) substrate; and (c) base contacts.

Fig. 6. Projection of a 10 μm wide section of the 3-D data plotted in Fig. 5(a) centered on 19.5 μm.

Fig. 5(b) and (c) shows the same for charge collection results obtained on the HBT substrate and base, respectively. Note that most of the hole charge is collected on the substrate. Also note that the sensitive area for charge collection on the substrate contact is similar to that for the collector, while that for the base is much smaller than either the collector or the substrate. (More detailed analysis of IBICC microbeam data and charge collection mechanisms in 5HP SiGe HBT can be found in [8].)
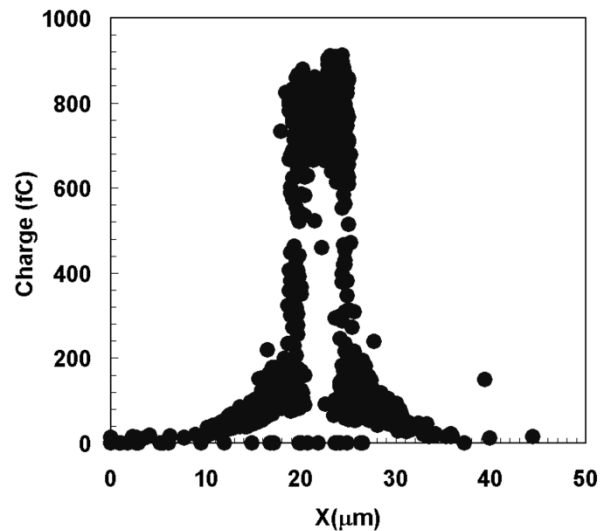
V. IMPLICATIONS OF BROADBEAM AND MICROBEAM RESULTS

A. Discussion of IBICC Results

We will focus our attention on the IBICC results for the collector contact; ion-induced collector current is the major mechanism that induces SEU for most standard SiGe HBT digital circuits [5]. (We note that the bias condition of $S_x = -5.2$ V on the substrate is the typical condition for nominal operation of HBT logic devices, while the E, B, and C grounded conditions are not typical. The IBICC technique can be used to quantitatively analyze the impact that events occurring outside the active and trench areas have on SEU. However, only qualitative information about SEU can be taken from events occurring inside these areas.)

The data plotted in Fig. 6 give a 10 μm wide slice in the X-direction (centered on Y $= 19.5$ μm) of the data plotted for collector IBICC events in Fig. 5(a). All data is projected onto the X-axis for this 2-D plot of the charge collected as a function of X position.

There are three well-defined regions along the x-axis that have very different charge collection characteristics. One, for x < 19 μm, shows a fall off in charge collected as the microprobe area was moved toward x $= 0$ μm; the same is true for x > 24 μm when the microprobe was moved toward larger x-values.

The third region is between x $= 19$ μm and x $= 24$ μm . The IBICC values across the third region are nearly the same. (There is some position dependent structure to the charge collection inside this region, which will be discussed in a few paragraphs after we identify the regions of the device that are responsible for each region of IBICC charge collection image.)

The distance along the X-axis between the outside edges of the deep trench is 5 μm. The isolation trenches are 1 μm wide and the active region is 3 μm long in this direction. Fig. 6 shows the device centered on x $= 22$ μm.

While it is impossible to identify the location of a single event to any better than a 2 μm^2 area (the microprobe spot size), it is clear from these data that the active region and trench region is contained between x $=\sim 19~\mu m$ and $\sim 24~\mu m$ (the trench region surrounds the active region and is $\sim 1~\mu m$ wide). It is also clear that most of the events outside this region are consistent with events that traverse the substrate region only. Since the microbeam ions were always normally incident, these data show that significant amount of charge is collected for events occurring as far away as 10-15 μm from the deep trench edge.

Finally, we take a closer look at the IBICC structure that occurs between x $= 19~\mu m$ and $24~\mu m$. There is an enhanced amount of charge collected for events that occur near the trench area (x $= 19~\mu m$ for example)—several ion strikes occurring near the deep trench area have IBICC values greater than 800 fC, while almost none of the events in the active area (x $= 22~\mu m$ for example) have values greater than 800 fC. Events occurring near the trench area can induce an enhancement factor over those events occurring in the active area. We are continuing to research this phenomena.

B. Charge Collection Mechanisms for SEU in the PRN

A limit on the critical charge for the PRN can be estimated by assuming a charge collection depth between 5 and 10 μm (this is consistent with 3-D device simulations on the 0.50 μm technology [8]). Using this and estimating from Fig. 3 that the threshold LET is probably $< 1.0~\mathrm{MeV-cm^2/mg}$, the upper limit for the critical charge for this device is less than 150 fC, and could be as low as 50 fC.

As can be seen in Fig. 6, the smaller charge collection events, which occur outside the active and trench areas have values > 75 fC for distances as far as 5 μm away from the deep trench. There is significant amount of charge collected by the collector contact from carriers that are generated in the substrate region beyond the trench—enough to cause an upset in several circuit types. The PRN described in this paper is one example. (Note that the biasing of the substrate for the microbeam data was consistent with the bias of the substrate for the PRN circuit.)

The active volume defines a portion of the SEU sensitive volume, the remaining portion of the sensitive volume is solely due to charge generated in the substrate volume and diffused into the active volume. This region extends away from the trench for several micrometers.

From a first-order modeling perspective, this multivolume structure significantly complicates the structure of the SEU sensitive volume. The sensitive volume is clearly no longer a simple RPP. It is rather simple to define the volume outlined by the trench and active volumes, but the details of the dimensions of the portion of the sensitive volume that is due to charge transport in the substrate will depend on the ion angle of incidence, the critical charge of the device, the ion's LET, and the diffusion length of the carriers in the substrate. This complex structure is one plausible explanation for the data trends observed in Fig. 3 and is a current area of research.

C. Analysis of SEU Cross-Section Dependence Using Classical RPP Assumptions

Even though the microbeam data show a very complex structure for charge collection and the SEU cross-section data show very abnormal trends, the need to have a conservative, relatively accurate on-orbit rate prediction approach demands that the first-order model of a thin RPP must be used, if possible, to describe data trends with LET and angle. In this section we will review the RPP assumptions and compare them to the data presented in this paper.

The data in Fig. 3 show that, for low LETs, there is an initial large drop in the cross section for angle between 0 and 45 degrees, this drop is followed by a slight increase as the beam angle is rotated from 45 to 72 degrees. These two factor show that the data in Fig. 3 cannot be fitted using a simple thin RPP model for the sensitive volume, which behaves as $1/\cos(\theta)$. (This was noted in [3] with regards to the IBM 5HP HBT technology.)

We also note that the measured cross section is greater than largest sensitive area than can be assume from the PRN circuit design and transistor area. The maximum valued for the sensitive volume can be estimated by summing up the total area enclosed by the trench and active areas for all possible sensitive transistors. Doing this and comparing it to the cross-section data in Fig. 3 for the highest LETs shows that the cross section is more than a factor of two greater than this area. Again supporting the fact that charge diffusing in the substrate volume is important for SEU and the RPP model fails to accurately estimate the device response.

One approach to describe "abnormal" SEU cross-section data that does not follow the simple thin RPP model is to argue that the analysis must include the difference in sensitivity due to edge effects for very thick sensitive volumes [see [13] for example]. The Heavy Ion Cross-section for single-event Upset (HIC-UP) model [13] has been used to account for edge effects in the RPP model.

The geometry of the IBM SiGe HBT requires that the 3-D aspects be included in any analysis. We have attempted to use the formulation described in [13] to predict the angular dependence of the heavy ion-induced SEU cross section presented in Fig. 3. We assumed a sensitive volume area of $5 \times 5~\mu m^2$ (the PRN was, for the most part, manufactured with $0.18 \times 3~\mu m^2$ long transistors that were confined in $5 \times 5~\mu m^2$ area that includes the active and trench areas.) We compared the data to the model for sensitive volume thickness that ranged from 5 to 10 μm (a range consistent with results from 3-D device physics modeling on the 0.50 μm technology [8]) in steps of 0.01 μm and critical charges that range from 0.1 fC to 200 fC in 0.1 fC steps. The "best fit" was found to be at a critical charge of 84.7 fC and a sensitive volume thickness of 5.00 μm. This best agreement (by eye) was between a factor of 1.06 (at 45 degrees) to a factor of 13.3 (at 70 degrees); an unacceptable fit when better than a factor of 10 is needed for on-orbit rate predictions.

Current implementations of the RPP model fail to predict the SEU cross-section trends with heavy ion beam angle. Current on-orbit rate prediction models, like CREME96 [10], that use RPP assumptions will give inaccurate estimates of the SEU rate, possibly by orders of magnitude.
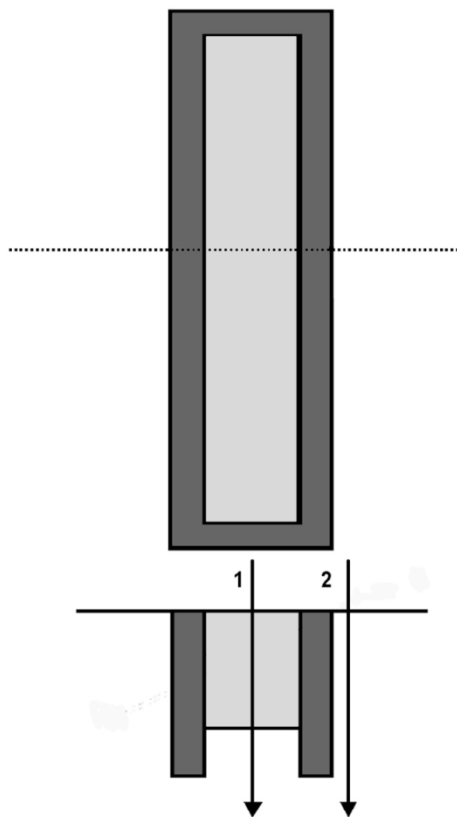
Fig. 7.   Top and cross-sectional view of trench.

Fig. 8.   REACT modeling (raw and normalized) compared to microbeam data.

VI. FIRST-ORDER MODELING OF MICROBEAM CHARGE COLLECTION

Charge collection in the test structure was modeled using the Monte Carlo treatment in a modified version of the Radiation Effects Array Charge Transport (REACT) code [11]. The model tracks carriers generated along the ion path until they are either collected in a high-field depletion region, recombine at a recombination surface, or exceed the carrier lifetime. The carriers are transported by diffusion and drift, including spatially varying electric fields, and those that reach a chosen surface are either counted or recombined.

Modeling with REACT was developed to do time efficient simulation of charge collection at a junction (typical single ion run in the current version takes less than an hour—we expect that later versions will cut this time by an order of magnitude or more). REACT is not intended to replace detailed device physics simulations like those in [7], [8], which can take several days to run a single ion. The intent is to build a model that can be used for fast calculation of sensitive volume charge collection that will replace the very rudimentary RPP modeling (like that used in CREME96 [10]).

The structure that was modeled is shown in Fig. 7. The interior region (light gray) represents a 3×21 μm^2 charge collection structure that is 5 μm thick. Any charge that is generated in this volume or generated outside the volume and then diffuses to the surface of the volume is assumed to be collected. Surrounding the charge collection region is a 1 μm wide oxide isolation trench (dark gray) that is 7 μm deep. Any charge generated in this volume or diffusing to the surface of this volume
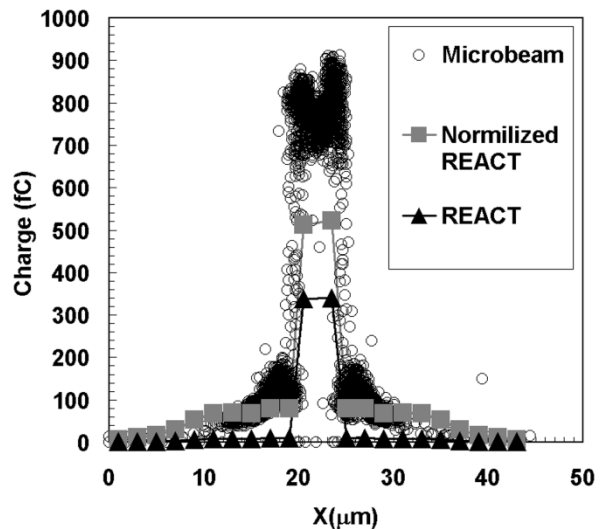
is recombined (we recognize that the current model cannot accurately predict the charge collection for events incident on the trench area, but because of the biasing condition used during IBICC testing, we are not attempting to be quantitative in predicting events inside the trench and active areas).

The regions outside the collection region and the isolation trench are assumed to have zero electric field and charge spreads from the ion track only by diffusion. A diffusion length of 15.8 μm, corresponding to a mobility of 1200 $cm^2/V-s$ and a lifetime of 80 ns, was assumed.

Modeling was carried out for cases 1 and 2 in Fig. 7, the ion penetrated the collection volume at normal incidence, at various locations along the dashed line in the top view in Fig. 7. For case 1 charge is collected by drift along the 5 μm path through the high-field region and then by diffusion from the zero-field region below. In case 2, the ion penetrated at normal incidence with an impact point "outside" but near the isolation trench. All of the charge is generated outside the structure. The charge that diffuses under the "wall" presented by the isolation trench is collected if the carrier reaches the bottom surface simulated collector region.

The results are shown in Fig. 8. (The microbeam data—unfilled circles—are plotted here for comparison.) The REACT output is plotted as the dark triangles. REACT predictions are an order of magnitude lower than the IBICC data for events outside the trench and active areas, and near a factor of two low for events in the active areas. The disagreement between REACT and the data could be due to the unknown mechanism that is causing the enhanced charge collection for events near the edge.

Fig. 8 also plots a version of the REACT output (filled squares) that is normalized to the microbeam events outside the area confined by the trench. This normalization was done by first subtracting of the contribution of modeled charge collected by drift in the collector region. Then the data was normalized to the events outside the area confined by the trench and added back to the drift component. This puts all simulation results to within a factor of two of the microbeam data. This result gives confidence that the charge collection trends as a function of position in the substrate volume can be accurately modeled by REACT.

VII. SUMMARY AND CONCLUSION

Digital circuits fabricated in IBM 0.20-μm (7HP) SiGe HBT technology can be very sensitive to SEU. The data presented in this paper represent the first measurement of the SEE sensitivity of a circuit fabricated in the 7HP process. These data demonstrated a very low threshold LET and the circuit response does not follow classical thin RPP or the less traditional thick RPP models.

IBICC microbeam data taken on the 7HP process shows that charge collection mechanisms for SEU are complicated by: 1) charge transport through the substrate and 2) a yet unexplained mechanisms for enhanced charge collection for events near the deep trench.

Combining the IBICC data with broad beam SEU data shows that the SEU sensitive area for IBM SiGe HBTs is a complex structure that includes the active area, the trench area, and possibly some portion of the substrate. The later component will be a function of the incident angle of the ion, its LET, and the critical charge at that specific node—a clear departure for the classical RPP modeling. This departure is also supported by the fact that that the measured PRN device cross section (at highest LETs) and the assumed sensitive area dimensions from transistor count and geometries differ by more than a factor of two. A first-order model was proposed and demonstrated moderate success for predicting IBICC results. This new modeling is a critical step toward development of an on-orbit rate prediction approach for HBT technologies.

ACKNOWLEDGMENT

REFERENCES

[1] J. D. Cressler and G. Niu, *Silicon-Germanium HBT's*. Norwood, MA: Artech House, 2002.
[2] [Online]. Available: http://www.mosis.org/Products/menu-products.html
[3] P. W. Marshall, M. A. Carts, A. Campbell, D. McMorrow, S. Buchner, R. Stewart, B. Randall, B. Gilbert, and R. A. Reed, "Single event effects in circuit-hardened SiGe HBT logic at gigabit per second data rates," *IEEE Trans. Nucl. Sci.*, vol. 47, pp. 2669–2674, Dec. 2000.
[4] G. Niu, R. Krithivasan, J. D. Cressler, P. Marshall, C. Marshall, R. Reed, and D. L. Harame, "Modeling of single-event effects in circuit-hardened high-speed SiGe HBT logic," *IEEE Trans. Nucl. Sci.*, vol. 48, pp. 1849–1854, Dec. 2001.
[5] G. Niu, R. Krithivasan, J. D. Cressler, P. A. Riggs, B. A. Randall, P. W. Marshall, R. A. Reed, and B. Gilbert, "A comparison of SEU tolerance in high-speed SiGe HBT digital logic designed with multiple circuit architectures," *IEEE Trans. Nucl. Sci.*, vol. 49, pp. 3107–3114, Dec. 2002.
[6] R. Krithivasan, J. D. Cressler, G. Niu, S. M. Currie, K. E. Fritz, P. A. Riggs, B. A. Randall, B. Gilbert, R. A. Reed, and P. W. Marshall, "An SEU hardening approach for high-speed SiGe HBT digital logic," *IEEE Trans. Nucl. Sci.*, vol. 50, pp. 2136–2144, Dec. 2003.
[7] G. Niu, J. D. Cressler, M. Shoga, K. Jobe, P. Chu, and D. L. Harame, "Simulation of SEE-induced charge collection in UHV/CVD SiGe HBT's," *IEEE Trans. Nucl. Sci.*, vol. 47, pp. 2682–2689, Dec. 2000.
[8] M. Varadharajaperumal, G. Niu, R. Krithivasan, J. D. Cressler, R. A. Reed, P. W. Marshall, G. Vizkelethy, P. E. Dodd, and A. J. Joseph, "3D simulation of heavy-ion induced charge collection in SiGe HBT's," *IEEE Trans. Nucl. Sci*, vol. 50, pp. 2201–2208, Dec. 2003.
[9] G. Vizkelethy, *Proc. 2002 NSREC Radiation Data Workshop Record*, Phoenix, AZ, 2002, pp. 165–170.
[10] [Online]. Available: https://creme96.nrl.navy.mil
[11] J. C. Pickel, R. A. Reed, R. Ladbury, B. Rauscher, P. W. Marshall, T. M. Jordan, B. C. Fodness, and G. Gee, "Radiation-induced charge collection in infrared detector arrays," *IEEE Trans. Nucl. Sci.*, vol. 49, pp. 2822–2829, Dec. 2002.
[12] A. Campbell, "Test Hardware," Naval Res. Lab., Washington, DC.
[13] L. W. Connell, F. W. Sexton, P. J. McDaniel, and A. K. Prinja, "Modeling the heavy ion cross-section for single event upset with track structure effects: The HIC-UP-TS model," *IEEE Trans. Nucl. Sci.*, vol. 43, pp. 2814–2819, Dec. 1996.